# Numerical Models of Boundary Layer Processes over and around the Gulf of Mexico during a Return-Flow Event

A. BIROL KARA, JAMES B. ELSNER, AND PAUL H. RUSCHER

*Department of Meteorology, The Florida State University, Tallahassee, Florida*

(Manuscript received 7 March 1997, in final form 14 July 1998)

ABSTRACT

The return-flow of low-level air from the Gulf of Mexico over the southeast United States during the cool season is studied using numerical models. The key models are a newly developed airmass transformation (AMT) model and a one-dimensional planetary boundary layer (PBL) model. Both are employed to examine the thermodynamic structure over and to the north of the Gulf. Model errors for predicting minimum, maximum, and dewpoint temperatures at the surface during both offshore and onshore phases of the return-flow cycle are analyzed. PBL model forecasts indicate soil moisture values obtained from the Eta Model improve accuracy. It is shown that forecasts of maximum temperature for coastal locations are sensitive to the soil moisture used in the PBL model. The AMT model performs well in determining boundary layer parameters since it includes horizontal advective processes. The AMT model is also able to predict the regional differences caused by different surface forcing while passing over land or sea. Results lead to a strategy for making predictions during cool-season return-flow events over and around the Gulf of Mexico.

## 1. Introduction

The low-level northward transport of moisture from the Gulf of Mexico associated with return flow on the backside of a retreating surface anticyclone can cause major problems for weather forecasters along the Gulf coast (e.g., Merrill 1992; Crisp and Lewis 1992). Return flow is the second half of a cycle that begins with an offshore flow. The return-flow cycle begins as classic airmass modification when cold and dry continental air tracks over a relatively warm ocean (offshore flow), but is distinguished from the classic modification process by synoptic conditions that cause the modified air to return to the land, as an onshore flow (Crisp and Lewis 1992).

The net results of the insufficient data and poor model physics are an improper simulation of the thermodynamic structure of the marine layer that returns to the continent (Weiss 1992). Once the return flow begins, advection becomes important, making the one-dimensional models less useful as a forecasting tool (e.g., Holtslag et al. 1990). Knowledge of sea surface temperatures (SSTs) and air parcel trajectories are necessary for making accurate weather forecasts during the cool-season return-flow events (e.g., Reiff et al. 1984; Lewis and Crisp 1992). Several mesoscale models have been developed to more accurately forecast the airmass modification during a return-flow event. Burk and Thompson (1992) have used the air mass transformation (AMT) model as a forecasting tool over the Gulf of Mexico. Advective processes dominate modification processes in the Nested-Grid Model (NGM) forecast as the cold-air outbreak spreads over the Gulf of Mexico, so airmass modification is not as important as advection in the NGM forecast as indicated in Janish and Lyons (1992).

In this paper, we focus on a newly developed three-dimensional AMT model for short-range weather forecasting of the atmospheric boundary layer (ABL) parameters around the Gulf of Mexico. We follow the work of Holtslag et al. (1990) and Sloan (1994) to develop a multilayer AMT model and examine return-flow events. The three-dimensional AMT model consists of a one-dimensional PBL model (Troen and Mahrt 1986) embedded within a trajectory model. The boundary layer as a part of the AMT model is described with K theory and countergradient transport terms (Troen and Mahrt 1986; Deardorff 1973). Section 2 is a summary of basic equations used in both the PBL and AMT models. Synoptic settings of a return-flow cycle are given in section 3. Model forecast errors are discussed in section 4. Summary and conclusions are provided in section 5. A list of symbols used in the paper is given in the appendix.

## 2. Boundary layer parameterizations

A high-resolution one-dimensional PBL model is coupled with an active two-layer soil model (Mahrt and

*Corresponding author address:* Birol Kara, Army Ammunization Plant, Sverdrup, Bldg. 9101, NASA/Stennis Space Center, MS 39529. E-mail: kara@nrlssc.navy.mil

Pan 1984) and a primitive plant canopy model (Pan and Mahrt 1987). The PBL model consists of a high-resolution grid. In this present study there are 70 levels from the surface to 10 000 m with a grid spacing of 20 m in the lowest 400 m, 50 m from 400 to 1400 m, and 100 m from 1400 to 2000 m (see also Troen and Mahrt 1986). Here a short summary of the model equations is given.

### *a. Model equations*

The model forecasts time tendencies due to turbulent mixing of specific humidity ($q$), potential temperature ($\theta$), and horizontal components of the wind ($u$ and $v$) as follows:

$$\frac{\partial V_h}{\partial t} = \frac{\partial}{\partial z}\left(K_m \frac{\partial V_h}{\partial z}\right) - w\frac{\partial V_h}{\partial z}, \tag{1}$$

$$\frac{\partial \theta}{\partial t} = \frac{\partial}{\partial z}\left[K_h\left(\frac{\partial \theta}{\partial z} - \gamma_\theta\right)\right] - w\frac{\partial \theta}{\partial z}, \tag{2}$$

$$\frac{\partial q}{\partial t} = \frac{\partial}{\partial z}\left(K_h \frac{\partial q}{\partial z}\right) - w\frac{\partial q}{\partial z}, \tag{3}$$

where $K_m$ and $K_h$ are the eddy diffusivities for momentum and heat, respectively, and $\gamma_\theta$ is the countergradient correction for potential temperature. Only the vertical diffusion terms due to boundary layer mixing and the vertical advection terms due to a prescribed vertical motion are considered in order to evaluate these equations. In Eq. (3) "$w$" is estimated using the method of O'Brien (1970). Horizontal wind components, specific humidity, and potential temperature are calculated at the computational levels while the derivatives of these parameters with respect to vertical coordinate ($z$) are calculated between computational levels.

Several formulations are suggested and discussed for eddy diffusivity in the literature (e.g., Zhang and Anthes 1982). A commonly used method is $K_h = l^2 S f(\mathrm{Ri})$. Here $l$ is an appropriate length scale for turbulent diffusion but erratic for unstable conditions (Wyngaard and Brost 1984). Formulation of $K_m$ is shown in Eq. (4) and the eddy diffusivity for heat ($K_h$) is expressed in terms of the turbulent Prandtl number (Pr):

$$K_m = w_s h k \frac{z}{h}\left(1 - \frac{z}{h}\right)^2, \tag{4}$$

$$\mathrm{Pr} = \left[\frac{\Phi_h(z/L)}{\phi_m(z/L)} + ck\frac{z}{h}\right]. \tag{5}$$

The Prandtl number is determined as the value at the top of the surface layer ($z = 0.1$ h) using surface similarity theory and taken as 1.0 for stable and neutral cases. It is also assumed independent of height above the surface layer. The nondimensional profile functions for the shear ($\Phi_m$) and temperature ($\Phi_h$) gradients are taken from Businger et al. (1971) with modifications by Holtslag (1987).

The countergradient term for potential temperature ($\gamma_\theta$) in Eq. (2) represents nonlocal influences on the mixing by turbulence and is neglected for a stably stratified boundary layer since the physical processes that cause turbulent transport are often quite different between stable and convective cases (Deardorff 1972, 1973). This countergradient term is described as follows:

$$\gamma_\theta = \begin{cases} 0 & \text{stable,} \\ c\dfrac{(\overline{w'\theta'})_s}{w_s h} & \text{unstable,} \end{cases} \tag{6}$$

where $(\overline{w'\theta'})_s$ is the surface flux of potential temperature. The velocity scale is parameterized as follows:

$$w_s = u_*(\Phi_m)^{-1}\left(\frac{z_s}{L}\right). \tag{7}$$

The surface temperature above the sea is nearly constant during the forecast period. In this case a profile method is used to derive the surface fluxes (Holtslag et al. 1990). Above land, surface fluxes are parameterized following Mahrt (1987) for the stable case and following Louis et al. (1982) for the unstable case (with modifications by Holtslag and Beljaars 1989). The length scale for the surface boundary layer is the classic Monin–Obukhov ($L$) length, and it is used in the nondimensional profile functions:

$$L = -\frac{\theta_{sv} u_*^3}{gk(\overline{w'\theta'})_s}. \tag{8}$$

Fractional cloud cover (CLC) is calculated using the following equation:

$$\mathrm{CLC} = f(\overline{\mathrm{RH}}, \sigma_{\mathrm{RH}}), \tag{9}$$

where $\overline{\mathrm{RH}}$ is the maximum relative humidity in the boundary layer and $\sigma_{\mathrm{RH}}$ is the standard deviation of relative humidity explaining the turbulent and subgrid mesoscale variations in relative humidity. The turbulent variability of relative humidity is formulated in terms of boundary layer similarity theory. With unstable conditions, boundary layer clouds first form at lower relative humidities compared to the stable case (Kara 1995; Holtslag et al. 1990).

### *b. Soil model*

The soil model is based on Mahrt and Pan (1984) and Pan and Mahrt (1987). The soil model does not account for horizontal variations in the soil. The soil model consists of a thin upper layer, 5 cm thick, and a thicker lower layer, 95 cm thick. For the nondimensional volumetric water content the soil hydrology is expressed as follows:

$$\frac{\partial \Theta}{\partial t} = \frac{\partial}{\partial z}\left[D(\Theta)\frac{\partial \Theta}{\partial z}\right] + \frac{\partial K(\Theta)}{\partial z}; \tag{10}$$

$D$ and $K$ are functions of the volumetric water content. Through the extremes of wet and dry soil conditions, the coefficients $D$ and $K$ can vary by several orders of magnitude; therefore, they cannot be treated as constants. The layer integrated form of Eq. (10) for the $i$th layer is

$$\Delta z_i = \left[D(\Theta)\frac{\partial \Theta}{\partial z} + K(\Theta)\right]_{z_{i+1}} - \left[D(\Theta)\frac{\partial \Theta}{\partial z} + K(\Theta)\right]_{z_i}. \tag{11}$$

This equation is valid for a layer $(z_i - z_{i+1}) = \Delta z_i$. At the surface of the soil, the evaporation is called the direct evaporation. For direct evaporation at the air–soil interface ($z = 0$),

$$E_{\text{dir}} = \left[-D(\Theta)\left(\frac{\partial \Theta}{\partial z}\right)_o - K(\Theta_o)\right](1 - \sigma_f) + I(1 - \sigma_f). \tag{12}$$

The evaporation can proceed at a potential rate ($E_p$) when the apparent soil moisture at the surface ($\Theta_{\text{sfc}}$) is greater than the air-dry value ($\Theta_d$), that is, when the soil is sufficiently wet (Pan and Mahrt 1987; Mahrt and Ek 1984).

The canopy evaporation of free water ($E_c$) and the canopy water content ($c^*$) are formulated as follows:

$$E_c = E_p \sigma_f \left[\frac{c^*}{S'}\right]^{n^*}, \tag{13}$$

$$\frac{\partial c^*}{\partial t} = \sigma_f \times \text{Precipitation} - E_c. \tag{14}$$

The model incorporates transpiration ($E_t$) in the following manner:

$$E_t = E_p \sigma_f k_v \frac{\sum_{i=1}^{2} [\Delta z_i g(\Theta_i)]\left[1 - \left(\frac{c^*}{S'}\right)^{n^*}\right]}{\sum_{i=1}^{2} [\Delta z_i]}. \tag{15}$$

The nondimensional transpiration rate is parameterized following Pan and Mahrt (1987) as follows:

$$g(\Theta) = \begin{cases} 1 & \Theta > \Theta_{\text{ref}}, \\ \dfrac{\Theta - \Theta_{\text{wilt}}}{\Theta_{\text{ref}} - \Theta_{\text{wilt}}} & \Theta_{\text{ref}} \geq \Theta > \Theta_{\text{wilt}}, \\ 0 & \Theta_{\text{wilt}} \geq \Theta. \end{cases} \tag{16}$$

The transpiration limit $\Theta_{\text{ref}}$ and $\Theta_{\text{wilt}}$ refer, respectively, to an upper reference value, which is the $\Theta$ value where transpiration begins to decrease due to a deficit of water, and the plant wilting factor, which is the $\Theta$ value where transpiration stops (Mahrt and Pan 1984). After consulting numerous studies $\Theta_{\text{ref}}$ is assigned a value of 0.25, and $\Theta_{\text{wilt}}$ is chosen to be 0.12 (e.g., Pan and Mahrt 1987).

Total evaporation is obtained by adding the direct soil evaporation, the transpiration, and the canopy evaporation as follows:

$$E = E_{\text{dir}} + E_c + E_t. \tag{17}$$

The surface specific humidity is calculated from

$$q_s = q_o + \frac{E}{\rho_o C_h}. \tag{18}$$

This quantity is the specific humidity at the surface that allows total evaporation to be calculated from the bulk aerodynamic relationship.

Soil thermodynamics are treated with a prognostic equation for soil temperature ($T$) such that

$$C(\Theta)\frac{\partial T}{\partial t} = \frac{\partial}{\partial z}\left[K_T(\Theta)\frac{\partial T}{\partial z}\right]. \tag{19}$$

The volumetric heat capacity ($C$) and the thermal conductivity of the soil ($K_T$) are both functions of the soil water content. In Eq. (19) C is linearly related to volumetric water content, whereas the coefficient of $K_T$ is a highly nonlinear function of volumetric water content and increases by several orders of magnitude from dry to wet soil conditions.

The layer integrated form of Eq. (19) is

$$\Delta z_i C(\Theta)\frac{\partial T_i}{\partial t} = \left[K_T(\Theta)\frac{\partial T}{\partial z}\right]_{z_{i+1}} - \left[K_T(\Theta)\frac{\partial T}{\partial z}\right]_{z_i}. \tag{20}$$

The upper boundary condition for the soil thermodynamic model is the soil heat flux, which is calculated as follows:

$$G = K_\Theta\left(\frac{\partial T}{\partial z}\right)_{z=0}. \tag{21}$$

The soil system is closed except for the potential evaporation. For the two-level soil model at 2.5 cm the following may be written:

$$\left(\frac{\partial T}{\partial z}\right)_{z=0} = \frac{T_s - T_{1\,\text{soil}}}{\Delta z}, \tag{22}$$

where $T_s$ is the skin temperature. Finally, surface temperature is calculated from the surface energy balance method:

$$(1 - \alpha)S\downarrow + L\downarrow - \sigma_b \theta_s^4 \uparrow = G\downarrow + H\uparrow + L_e \times E\uparrow, \tag{23}$$

where each term is expressed in watts per square meter (W m$^{-2}$). In this equation $\alpha$ is the surface albedo and is a function of surface characteristics, $S$ is downward atmospheric radiation, $G$ is soil heat flux, and $E$ is the total evaporation. Sensible heat flux is parameterized as

$H = \rho_o C_p C_h(\theta_s - \theta_o)$. Other parameters are shown in the appendix. Details of the surface energy balance equation [Eq. (23)] and surface layer parameterizations can be found in Troen and Mahrt (1986).

### c. Computational procedures

The first step is to calculate the external forcing of the incoming solar radiation reduced by a fractional cloud cover. Fractional cloud cover computed from profiles of temperature and moisture from the previous time step is used for calculation of downward atmospheric radiation. With Eq. (21), the soil heat flux is obtained using the soil thermodynamic model from Eq. (20). In the finite difference form of Eq. (22), the skin temperature ($T_s$) appears as an unknown. The only variables needed to close the surface layer model are surface specific humidity ($q_s$) and surface potential temperature ($\theta_s$). They are available from the soil model and the surface energy balance calculation, respectively. Having obtained $q_s$ and $\theta_s$, the surface layer parameterization is used to obtain the surface stress, surface fluxes. Moreover, the Monin–Obukhov length and the similarity diffusivity profiles ($K_h$ and $K_m$) for the surface layer are calculated. The nondimensional profile functions for shear and thermal gradients are then computed in addition to diffusivity coefficients above the surface layer. Finally, the tendencies of wind velocity, potential temperature, and specific humidity are calculated from Eqs. (1)–(3).

### d. Description of the AMT model

The PBL model as part of the AMT model describes the evolution of temperature and moisture resulting from the exchange of heat, water vapor, and momentum at the earth's surface as well as from the entrainment of air above the ABL. Over sea, surface temperature and wind speed determine the transfer of heat, water vapor, and momentum to the boundary layer. As in the one-dimensional PBL model, the AMT model can be used on a daily basis because it uses routine weather data. The trajectory model, which consists of air parcel trajectories, input soundings, the land–sea mask and SST are described here. Details on how advection is included in the AMT model may be found in Holtslag et al. (1990).

The absence of upper-air observations over the Gulf of Mexico makes it difficult to get reliable three-dimensional trajectories. In general, forecast fields from numerical models are not very accurate, and the vertical motion from the NGM is questionable (Janish and Lyons 1992). The AMT model needs trajectory information at 975, 850, and 700 mb. Since there are not other alternatives of calculating trajectories, forecast and analyzed wind fields of a larger-scale numerical model are used to calculate backward trajectories in time, starting from the receptor (end) point to the source area by using National Centers for Environmental Prediction observations. Lowest trajectories are at a height of about 200 m and the highest are below 700 mb. In the source area the observations of two or three nearest radiosonde stations are used to construct initial profiles of potential temperature and specific humidity (Reiff et al. 1984). Input data are transformed from pressure coordinates to sigma ($\sigma$) coordinates, where $\sigma$ is defined as a ratio of pressure to the actual surface pressure of each radiosonde. The original sounding in the source area is defined by a set of significant levels. These levels are interpreted by the inflection points of the profiles. All significant levels of input soundings are then used as significant levels for the analyzed sounding to make the initial profile. The values of temperature, pressure, moisture, and wind components are obtained from the input soundings by using a weighting procedure on a given sigma level in the horizontal as in Reiff et al. (1984). The analyzed sounding is then interpolated onto the model grid using a least squares minimization method.

To calculate surface fluxes, it is necessary to know if the AMT model is over land or water as it is being advected along the low-level trajectory. It was determined that with a time step of 3 min, a resolution of 0.1° would be accurate enough to show details of the coastline in the return-flow region. Most of the details of the coastline are well represented by the mask. Sea surface temperatures are needed as a prescribed bottom boundary condition when the model is determined to be over water. These temperatures are obtained weekly and are a blend of measurements and satellite-derived observations on a 1° grid. However, before the analysis is computed, the satellite-derived dataset is adjusted for biases as described in Reynolds (1988).

## 3. Synoptic setting of the case

### a. Vertical structure of the return-flow cycle

Several coastal and inland locations around the Gulf of Mexico are used to examine vertical structure of the return-flow cycle (Fig. 1). The coastal stations are Brownsville (BRO), Corpus Christi (CRP), Tallahassee (TLH), and Tampa Bay (TBW). Inland stations include Lake Charles (LCH), Jackson (JAN), and Shelby County Airport (BMX). Three buoy stations (B1, B2, and B3) are considered over the continental shelf of the Gulf to follow evolution of SST, air–sea temperature difference and wind speed. However, the analysis is only shown for B2, a nearshore location (see section 3b). Depth of the Continental Shelf at buoys B1, B2, and B3 is 40 m, 9 m, and 34 m, respectively.

Wind fields at 950 mb from the Rapid Update Cycle gridded data were analyzed to determine offshore and onshore phases from 1 January to 31 March in 1996. Wind fields from 12-h coastal upper-air soundings and those from Eta Model were also taken advantage of in

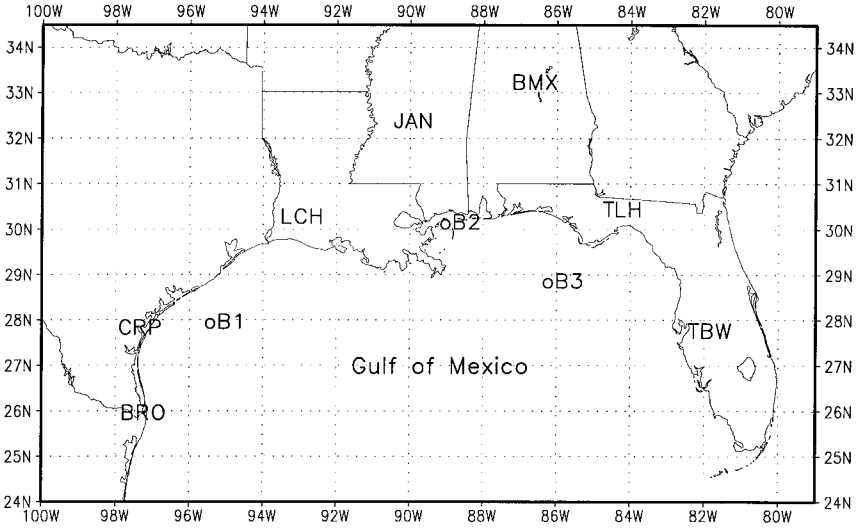


FIG. 1. Locations of coastal stations and inland stations around the Gulf of Mexico considered in this study. Buoy stations (B1, B2, and B3, whose national station identification numbers are 42019, 42007, and 42039, respectively) located over the Continental Shelf are also marked.

this determination. Specifically, the 2–9 February return-flow case was selected to examine cross sections of potential temperature and mixing ratio during a return-flow cycle (Fig. 2). These cross sections were obtained by using 12-h upper-air soundings from the surface to 500 mb. As seen from the coastal locations on the Texas coast, offshore flow, which started at 1200 UTC 2 February 1996, lasted until 0000 UTC 5 February when the onshore flow began. On the Texas coast CRP had little vertical wind shear (approximately below 800 mb) when the observed wind speeds from the buoy stations ($\approx$6 m s$^{-1}$) over the northwest Gulf replaced these winds on 5 February. Analysis of the wet-bulb temperatures showed the ground temperatures at inland locations (such as JAN and BMX) were cool relative to the returning Gulf air. The entire return-flow cycle lasted approximately 7 days, beginning over the Texas coast on 1200 UTC 2 February and ending 0000 UTC 9 February. Significant low-level moisture is absent along the Texas coast during the offshore phase. Moisture appears at CRP with easterly winds at 0000 UTC 5 February and increase slowly with the onset of the onshore flow. The near-surface moist layer begins as a narrow region of maximum mixing ratio value (4 g kg$^{-1}$) at CRP by 1200 UTC 5 February and expands eastward with time. The surface moist layer also deepens with time from a thickness of approximately 40 mb at 0000 UTC 6 February to a thickness of almost 200 mb at 1200 UTC 7 February, just ahead of the next cold front (not shown).

The stations used in the cross-section analyses are spread apart, inhibiting a clear picture of mesoscale moisture structures. Therefore, cross sections using the Eta Model initialized at 0000 UTC 3 February, during the offshore flow phase, are also examined. The cross-section analysis (Fig. 3) shows greater moisture over the sea with mixing ratio values ranging from 6 to 14 g kg$^{-1}$. Potential temperatures at the surface decrease with time while a small increase in the mixing ratio is observed over land. Moisture extends as high as 700 mb with a value of 2 g kg$^{-1}$ on 4 February just before onshore flow started. Once the return-flow begins (0000 UTC 5 February), and the parcel turns back toward the north, an increase in mixing ratio occurs with a value of approximately 8 g kg$^{-1}$ at 850 mb over land. It is noted that as the air moves across the Gulf, it continues to absorb heat and moisture at a very slow rate. In this cross-section analysis, the Eta Model exhibits good thermodynamic gradients across the Gulf of Mexico, unlike the typical NGM as shown by Janish and Lyons (1992).

### *b. Time series analysis over the Gulf*

Temperature differences between air and sea decrease slowly as the air returns to land, but some warming and moistening of the marine boundary layer occurs until the air traverses the colder shelf during return-flow events (Merrill 1992). Sea surface temperature usually acts as a lower boundary condition on the air that typically tracks southward. Therefore, evolution of SST over the continental shelf of the Gulf is needed. The time series of air–sea temperature difference ($T_a - T_s$) and wind speed (WS) at B2 from 1 January to 31 March are shown in Fig. 4 (top two panels). Strong wind speeds over the continental shelf of the Gulf usually corresponded to large air–sea temperature differences during this 3-month period (Fig. 4, and bottom panel). For instance, temperature differences ($T_a - T_s$) are less than $-1.7$°C when wind

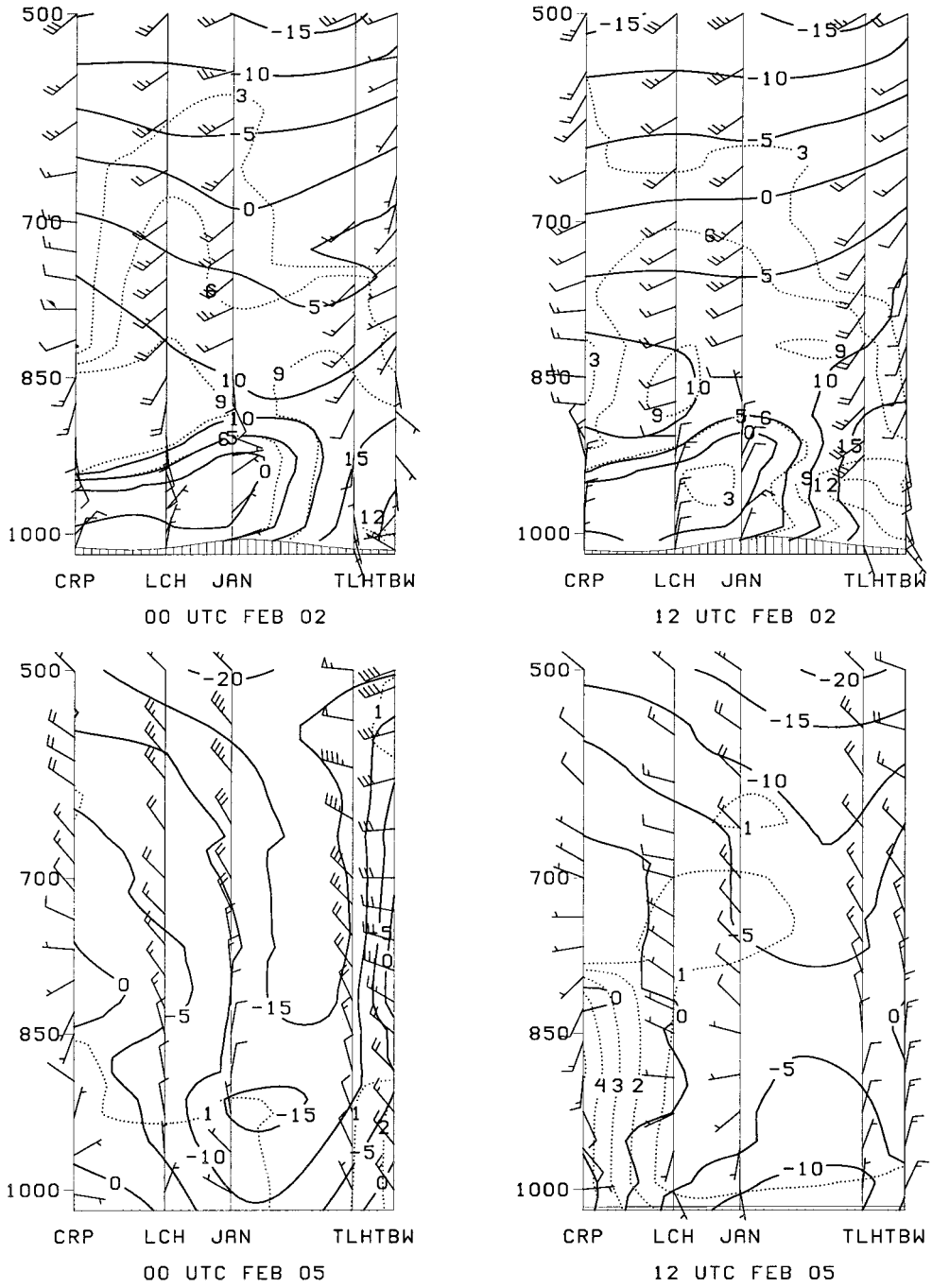


FIG. 2. Alongcoast cross sections of potential temperature ($\theta$) in °C (solid lines) and mixing ratio ($w$) (contours are dotted with intervals of 3 g kg$^{-1}$) at 0000 and 1200 UTC on 2 Feb (top panels). (Bottom panels) The same analysis for 5 Feb but increment of mixing ratio contours is 1 g kg$^{-1}$. Selected winds (m s$^{-1}$) are also plotted at each station.

speeds are greater than 10.5 m s$^{-1}$ except for 18 January when the positive air–sea temperature difference ($\approx$2°C) is observed during the onshore flow. Conditions when significant peaks of both air temperature and wind speed appeared are approximately WS $>$ 8.5 m s$^{-1}$ and $T_a - T_s < -3.0$°C except for 22 January when a very small positive air–sea temperature difference (0.5°C) and nearly calm wind (4.5 m s$^{-1}$) occurs. No significant peak is found for temperature when WS $<$ 8 m s$^{-1}$. These peaks usually occur during off-

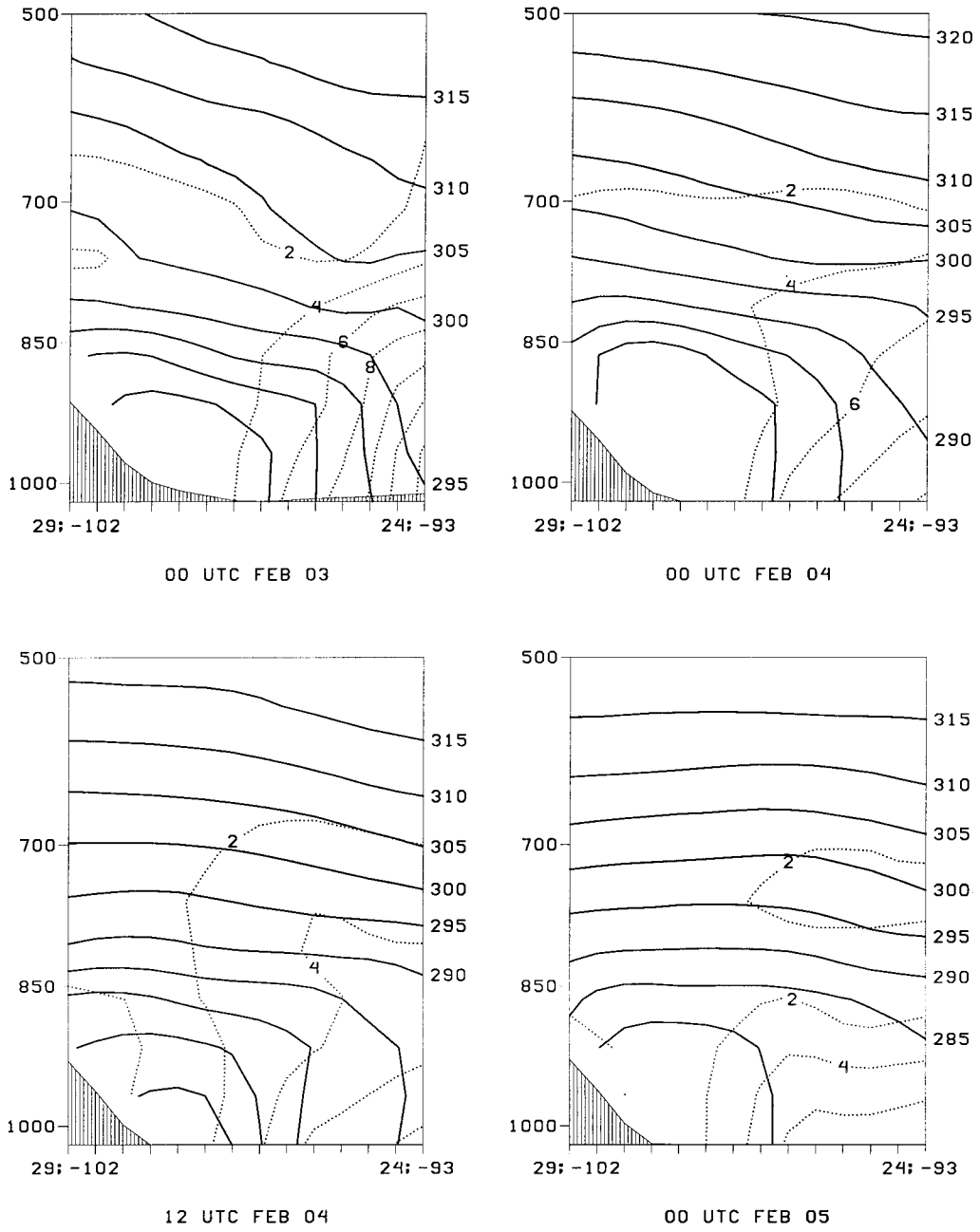


FIG. 3. Cross section of potential temperature ($\theta$) in kelvins (solid lines) and mixing ratio ($w$) in g kg$^{-1}$ (dotted lines) along the Gulf Coast. The values are obtained from the Eta Model initialized at 0000 UTC 3 Feb between a location on the Texas coast (29°N, 102°W) and a location on the Continental Shelf (24°N, 93°W).

shore flow when turbulence is dominant as explained in Lewis and Martin (1996), Lewis et al. (1997), and Kara (1996). However, during onshore flow, the marine layer becomes warmer than the underlying shelf water. Therefore, air–sea temperature differences tend to be smaller. During the observational period, there were four cases when peaks of both wind speed and air temperature occur simultaneously and nine cases with peaks only in the wind speed.

## 4. Model analyses

### *a. The PBL and AMT model forecasts*

Several parameters must be specified in the PBL and AMT models before a forecast can be made. Soil moisture and soil type are the most important of these parameters. Direct soil moisture measurements were not available for any coastal or inland locations around the Gulf; therefore, we obtained soil moisture values from

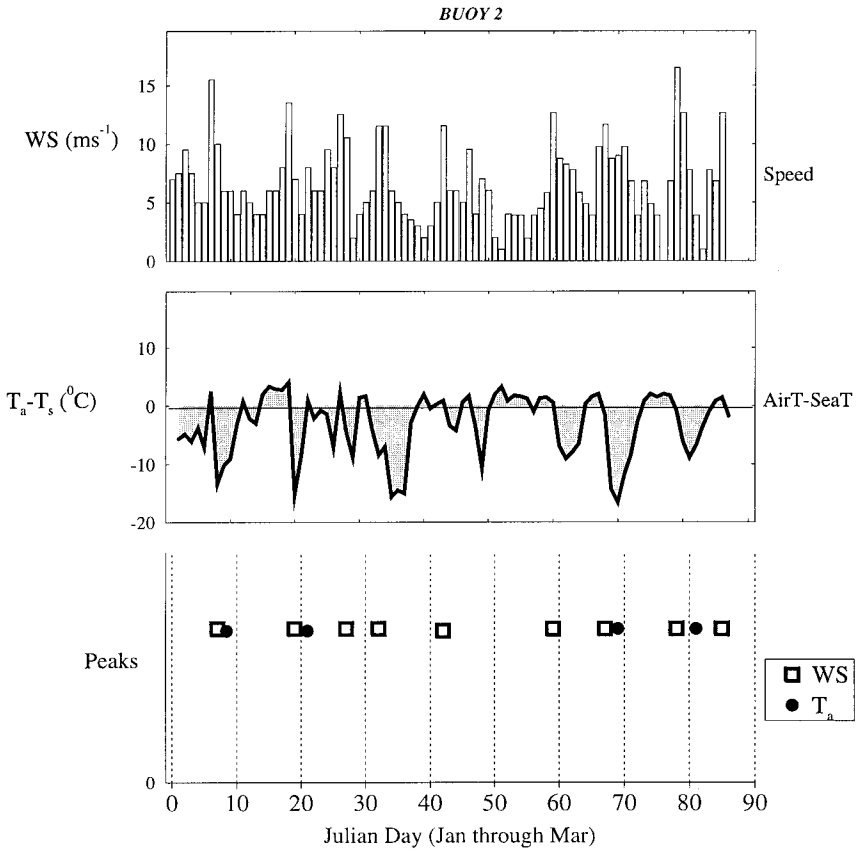


FIG. 4. Time series of wind speed (WS) in m $s^{-1}$ (top) and air–sea temperature difference ($T_a - T_s$) in °C (middle) at buoy 2 from January through March 1996. (Bottom) Open squares indicate cases when only peaks in wind speed occurred, and filled circles when significant peaks of both wind speed and air temperature occurred simultaneously.

the forecast cycles of the Eta Model for each station (see Fig. 5). Soil moisture values are nearly constant in March for each station after an increase starting approximately after 15 February. It is also important to remember that return-flow events, where significant moisture comes from the Gulf during the onshore phase, occur during this time of year.

It is possible to use a grid-scale weighting technique to determine soil type, but this requires an accurate dataset of soil type for the region (Avissar and Pielke 1989). In this study, soil types for each station are determined based on a general soil-type map depicted in Foth and Schafer (1980). Soil survey maps of the U.S. Department of Agriculture have also been consulted for this determination. Accordingly, soil types are clay loam for BRO, CRP, LCH; clay for JAN and BMX; and sandy clay loam for TLH and TBW (see Fig. 5). The soil properties for these types are similar to those used in the Eta Model (e.g., Zobler 1986; Black 1994), although we cannot exclude the possibility of some sensitivity here since different soil physics formulations are used in the two models. In addition to soil moisture and soil type the initial values for roughness lengths for heat and momentum are the same with a value of 0.01 m for each forecast although the model is sensitive to the value of roughness length used (Kara et al. 1998a; Kara et al. 1998b). The air-dry value is taken as 0.25 (Pan and Mahrt 1987). The initial value for albedo is 0.23 for each station (Stull 1983). By using these initial values, a 24-h lead forecast initialized with 1200 UTC sounding of the previous day is executed to find minimum temperature. A 24-h lead forecast initialized with 0000 UTC sounding of the current day is executed to find maximum temperature. In the same manner a 12-h and a 24-h lead forecast are also performed to find minimum and maximum temperature. The model forecasts are performed for each coastal and inland location. This analysis is discussed in section 4b.

Two different experiments are used to explain the effect of soil moisture on temperature estimates. First, the soil moisture is kept constant at 30% in all model forecasts performed for those days from January through March in 1996. Second, the soil moisture values extracted from the Eta Model for each day are used in the model forecasts. Figure 6 clearly shows the soil moisture values extracted from the Eta Model for TLH

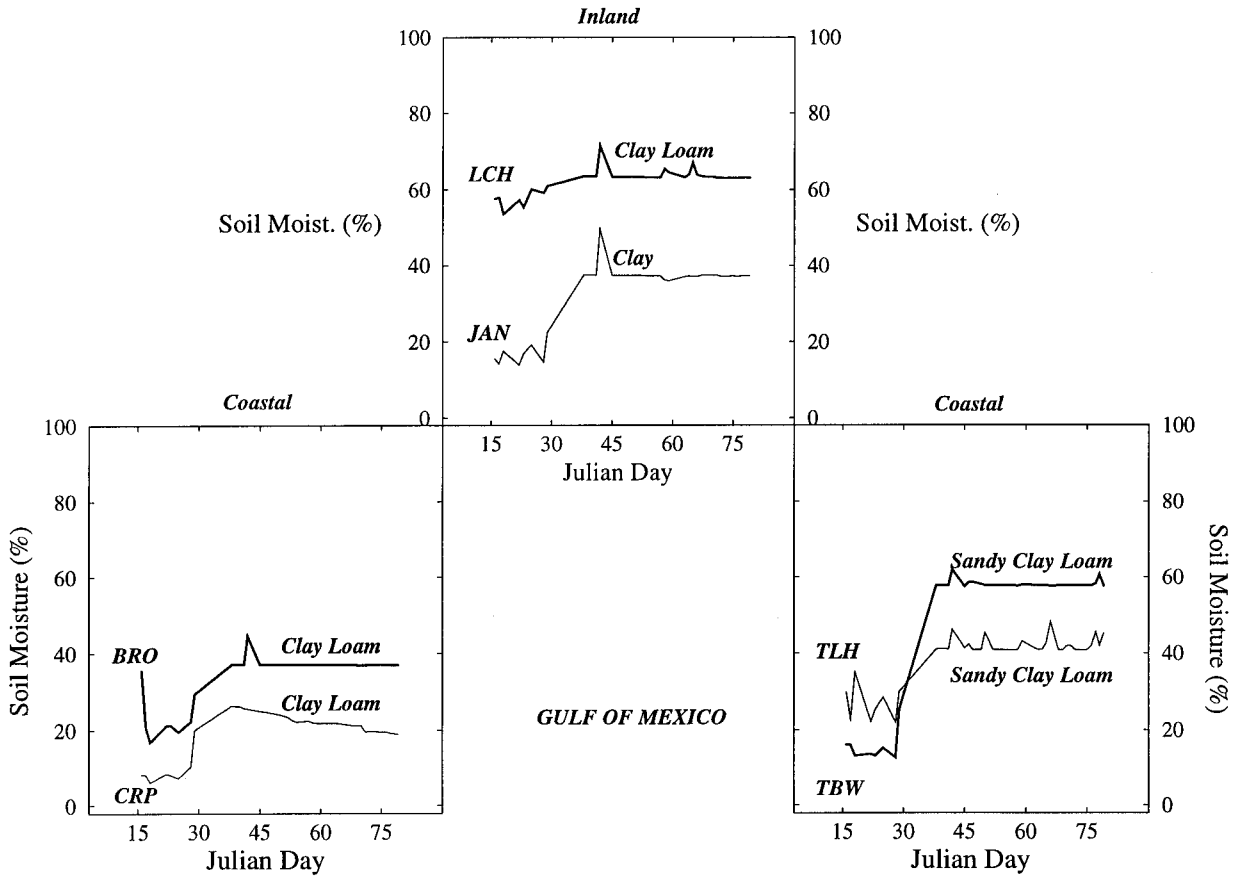


FIG. 5. Soil moisture values expressed as a percentage obtained from the Eta Model for both inland and coastal stations around the Gulf during Jan–Mar 1996. Soil types are also indicated.

do not substantively affect the difference between model and observed temperature. The intercomparison of model forecasts yields a correlation coefficient of 0.93. In contrast, forecasts of maximum temperature for CRP are more sensitive to the soil moisture values since the correlation coefficient between the temperature differences is only 0.71. As seen from Fig. 6, soil at CRP is much drier than the one at TLH, which helps to explain the greater sensitivity to soil moisture. Further comparisons concerning characteristics of the atmospheric boundary layer between the coastal and inland locations around the Gulf of Mexico can be found in Kara and Elsner (1999).

Forecasts of minimum temperature and dewpoint temperature are also examined in terms of the advective influence from air moving over the Gulf and land to investigate the AMT model performance. For model forecasts BRO, located on the southern Texas coast, is chosen. Brownsville is approximately 40 km from the Gulf of Mexico and this distance is important for advective effects over the location when one uses the AMT model. In our analyses, cases with advection from the Gulf are defined as $\geq$3 h of advection over sea during the previous 6 h of advection, as was done by Reiff et al. (1984). In other words, whether the air is moving over sea or land was determined using the trajectory information. Several cases including both land and air advection during the 24-h period were excluded from the statistical analyses.

The forecast is performed by starting the model over the Gulf and letting it arrive in BRO 24 h later. Even though the PBL model is sensitive to the amount of soil moisture used, it is not important in the AMT model since the low-level flow always originates over the Gulf. For each forecast, model minimum temperatures and dewpoint temperatures are compared with observed values. Table 1 shows that about 54% of the cases are advected over sea. Minimum temperature forecasts have a correlation coefficient of 0.82 for cases with advection from sea and 0.89 for cases with advection over land. Dewpoint temperature forecasts also show good results with a correlation coefficient of 0.83 during the land advection. Note that dewpoint temperatures are determined at the same time the minimum temperature is predicted. The mean error (me) values shown in Table 1 are calculated using $(M_f - M_o)/n$, where $M_f$ and $M_o$ are forecast and observed values, respectively. The mean errors are generally between 2° and 3°C.

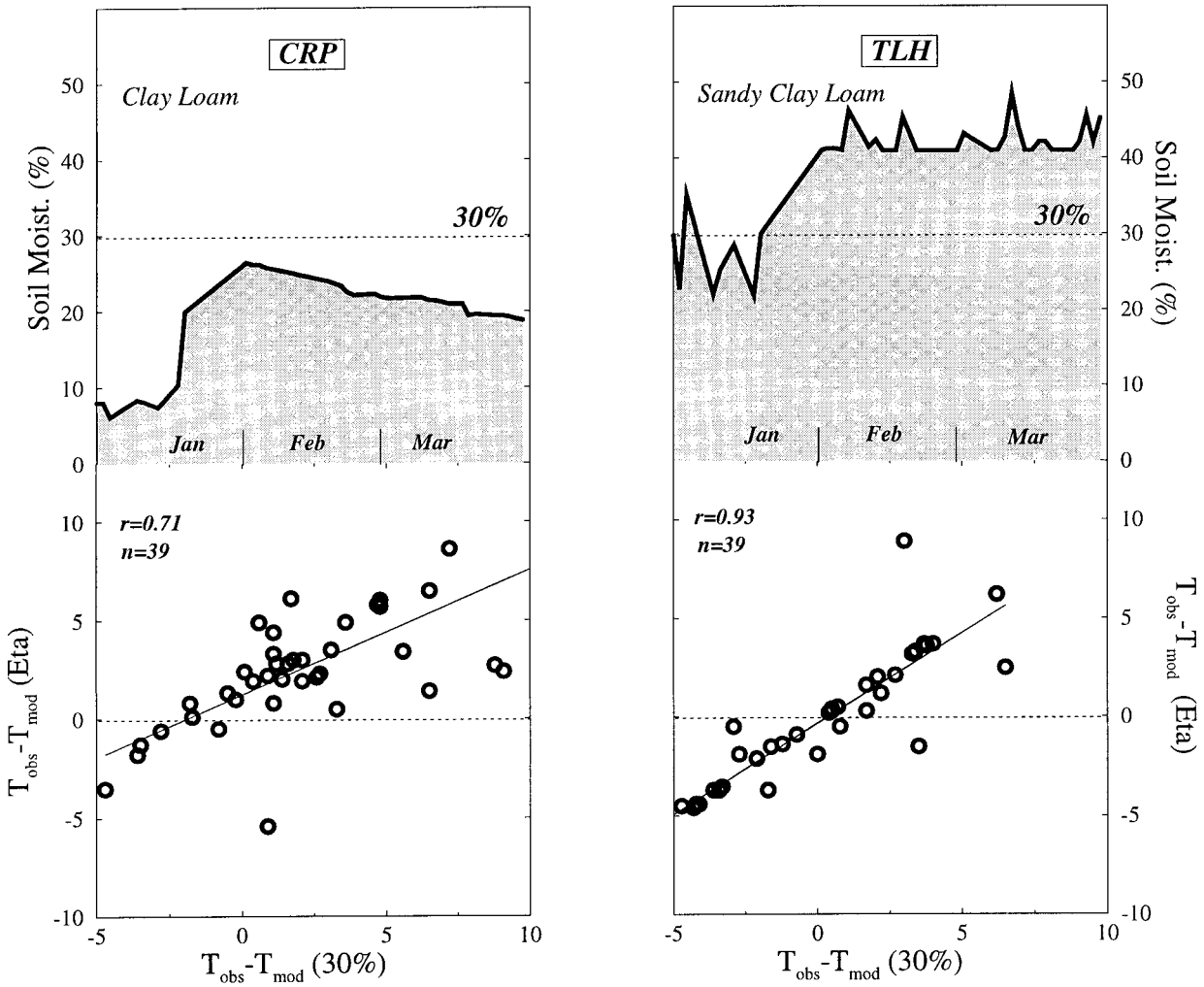


FIG. 6. (Top panels) Soil moisture values as a percentage from January through March 1996 for CRP and TLH. (Bottom panels) Comparisons of differences between observed and forecast maximum temperatures when constant 30% soil moisture values [$T_{obs} - T_{mod}$ (30%)] are used, and when soil moisture values obtained from the Eta Model [$T_{obs} - T_{mod}$ (Eta)] are used in the model forecasts.

### *b. Model forecast errors*

Given the error, $M_f - M_o$, between forecast and observed values, some statistics may be defined, such as bias, root-mean-square error (rmse), and correlation coefficient ($r$), as follows:

$$\text{bias} = \overline{M_f - M_o}, \tag{24}$$

$$\text{rmse} = \sqrt{\frac{\sum (M_f - M_o)^2}{n}}, \tag{25}$$

$$r = \frac{\sum M_f M_o}{n}. \tag{26}$$

TABLE 1. Correlation coefficients ($r$) and mean errors (me) between AMT model forecasts and observed values of minimum temperatures ($T_{min}$) and dewpoint temperatures ($T_d$). Forecasts, based on the model, started over the Gulf of Mexico and arrived at BRO 24 h later, are evaluated in categories with advection over land or advection over sea. The number of cases ($n$) is also shown for each category.

| Forecast (°C) | Advection type | $n$ | $r$ | me (°C) |
|---|---|---|---|---|
| $T_{min}$ | Over land | 18 | 0.89 | 2.3 |
| $T_{min}$ | From sea | 15 | 0.82 | 2.8 |
| $T_d$ | Over land | 18 | 0.83 | 2.5 |
| $T_d$ | From sea | 15 | 0.81 | 2.8 |

Model error statistics are computed from normalized values of $T_{mod}$ and $T_{obs}$ by subtracting the mean and dividing by the standard deviation, $M_i = (T_i - \overline{T_i})/\sigma_i$, where $i$ = mod or obs.

Tables 2 and 3 show the values of $r$ and rmse calculated station by station under each forecast category for minimum and maximum temperatures, respectively. As seen, rmse decreases with increasing correlation coefficients for each forecast category. The highest rmse values are found for the 36-h forecasts. In these cases, correlation coefficients changing from $r = 0.37$ at TBW

TABLE 2. Correlation coefficients ($r$) and rmse in °C between minimum temperatures obtained from the model and observed minimum temperatures. The number of cases (model forecasts performed) is 39 for each station and each forecast category.

| Forecast | | BRO | CRP | LCH | JAN | BMX | TLH | TBW |
|---|---|---|---|---|---|---|---|---|
| 12-h | $r$ | 0.85 | 0.91 | 0.92 | 0.91 | 0.91 | 0.88 | 0.82 |
| | rmse | 0.54 | 0.42 | 0.41 | 0.42 | 0.43 | 0.49 | 0.60 |
| 24-h | $r$ | 0.74 | 0.71 | 0.65 | 0.66 | 0.57 | 0.70 | 0.61 |
| | rmse | 0.72 | 0.76 | 0.84 | 0.82 | 0.92 | 0.77 | 0.88 |
| 36-h | $r$ | 0.48 | 0.50 | 0.47 | 0.72 | 0.70 | 0.52 | 0.37 |
| | rmse | 1.02 | 0.99 | 1.03 | 0.74 | 0.78 | 0.98 | 1.20 |

TABLE 3. Correlation coefficients ($r$) and rmse in °C between maximum temperatures obtained from the model and observed maximum temperatures. The number of cases (model forecasts performed) is 39 for each station and each forecast category.

| Forecast | | BRO | CRP | LCH | JAN | BMX | TLH | TBW |
|---|---|---|---|---|---|---|---|---|
| 12-h | $r$ | 0.85 | 0.82 | 0.81 | 0.82 | 0.85 | 0.82 | 0.67 |
| | rmse | 0.55 | 0.61 | 0.62 | 0.60 | 0.54 | 0.61 | 0.81 |
| 24-h | $r$ | 0.70 | 0.80 | 0.71 | 0.92 | 0.92 | 0.85 | 0.80 |
| | rmse | 0.77 | 0.63 | 0.77 | 0.41 | 0.40 | 0.55 | 0.63 |
| 36-h | $r$ | 0.62 | 0.64 | 0.57 | 0.66 | 0.71 | 0.78 | 0.79 |
| | rmse | 0.87 | 0.85 | 0.93 | 0.82 | 0.76 | 0.66 | 0.64 |

to $r = 0.72$ at JAN are relatively small. In general, 12-h and 24-h forecasts for minimum temperatures give better results since the values of $r$ are higher than 0.6 for each coastal and inland station except for BMX. Correlation coefficients start to increase slightly from the stations on the Texas coast to inland locations (JAN, BMX) and again decrease at stations on the Florida coast except for the 24-h minimum temperature forecasts. On the other hand, the minimum temperature estimates for 24-h forecasts occurred at night since the model was initialized the day before at 1200 UTC. Therefore, these forecasts are not as good as the 12-h forecasts. It is clear that the most reliable forecasts are over a 12-h period for the minimum temperature and over a 24-h period for the maximum temperatures.

A final comparison on the model performance is done by grouping all temperature forecasts together under a single category; that is, forecasts for all stations and over all forecast periods (12-h, 24-h and 36-h) are accumulated. There are a total of 1638 model forecasts. Figure 7 involves the class intervals for the temperature differences between observed and forecast values and gives some statistical results for this analysis. In general, the PBL model is able to predict the temperatures within a small error. More than half of the temperatures obtained from the model (58.1%) are warmer than the observed temperatures. The correlation coefficient between all model temperatures and observed temperatures is 0.78 with an rmse of 0.64°C and a bias of 0.53°C. The mean of all model temperatures is 15.7°C, which is very close to the observed mean temperatures of 15.1°C. The combined statistics indicate overall good agreement between the model results and observations.

## 5. Summary and conclusions

The interaction between oceanic cooling and airmass modification is important to weather forecasting along the coastal plain of the Gulf of Mexico. Northward transport of moisture on the back side of a retreating surface anticyclone can make forecasting difficult for locations along the coastal states. Since operational numerical models generally perform poorly during a return-flow cycle, we developed a three-dimensional airmass transformation (AMT) model that consists of a one-dimensional PBL model embedded in a three-dimensional trajectory model. Horizontal advective processes incorporated within the AMT model yielded better forecasts than the one-dimensional PBL model itself. As expected, the results are sensitive to the position of the land–sea transition of the calculated trajectory. The AMT model clearly shows an ability to accurately forecast surface temperatures. We also found that forecasts of maximum temperature for the coastal locations are more sensitive to the soil moisture values in the PBL model in comparison to inland locations. Further study is necessary to fully determine the effectiveness of the AMT model. Stations around the Gulf of Mexico do not always report data. This causes difficulties in the construction of the initial profile for the model. The first step toward improving the model would be a more realistic input sounding. One solution may

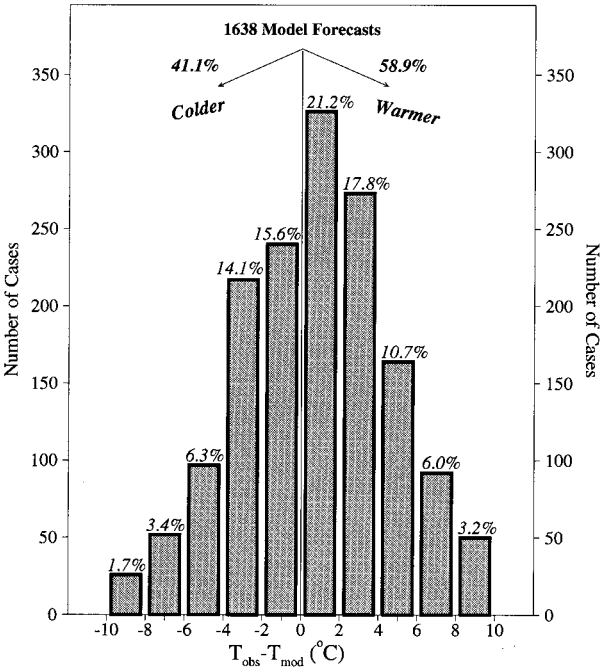


FIG. 7. Number of cases vs (observed–model) temperatures for all model forecasts (12-h, 24-h, 36-h) involving both maximum and minimum temperatures. The percentage of each category is written above the bars.

be to use a large-scale model sounding at the grid point over the Gulf instead of using station soundings. This will probably improve the model initialization and subsequent forecasts. For this study we are examining sensitivity to soil moisture; however, for operational studies, we should use the best available estimate of soil moisture. Unfortunately, reliable measurements of soil moisture are sparse. In the future, Doppler radar estimates of precipitation could be related to soil moisture in a meaningful way.

*Acknowledgments.* This research was partially supported by the U.S. Air Force Office of Scientific Research under Contract F19628-93-K-0006. The helpful comments of Dr. K. A. Kloesel and Dr. T. N. Krishnamurti (both at The Florida State University) at different stages of this research are greatly appreciated. We would like to extend our special thanks to Dr. J. M. Lewis of the National Severe Storm Laboratory, in Oklahoma, for providing very useful explanations about return-flow events. Mr F. Zhao is thanked for providing computer assistance in terms of model modification. Much appreciation is extended to the reviewers for their helpful comments, which significantly improved the quality and readability of this paper.

## APPENDIX

### List of Symbols

| | |
|---|---|
| $c^*$ | Canopy water content (m $s^{-1}$) |
| $c$ | A nondimensional constant (8.5) |
| $C$ | Volumetric heat capacity ($1.26 \times 10^6$ W $m^{-3}$ $K^{-1}$ for soil) |
| $C_h$ | Exchange coefficient for moisture (m $s^{-1}$) |
| $C_p$ | Specific heat (1004.5 J $kg^{-1}$ $K^{-1}$) |
| $D$ | Coefficient of diffusivity ($m^2$ $s^{-1}$) |
| $E_t$ | Transpiration (m $s^{-1}$) |
| $E_{\text{dir}}$ | Direct evaporation (m $s^{-1}$) |
| $g$ | Gravitational acceleration (9.8 m $s^{-2}$) |
| $h$ | Atmospheric boundary layer height (m) |
| $I$ | Infiltration rate (m $s^{-1}$) |
| $k$ | von Kármán constant (0.4) |
| $K$ | Hydraulic conductivity (m $s^{-1}$) |
| $K_T$ | Thermal conductivity |
| $K_h$ | Eddy diffusivity for heat ($m^2$ $s^{-1}$) |
| $K_m$ | Eddy diffusivity for momentum ($m^2$ $s^{-1}$) |
| $k_v$ | Plant resistance factor (between 0 and 1) |
| $L_e$ | Latent heat of vaporization ($2.5 \times 10^6$ J $kg^{-1}$) |
| $M_f$ | Normalized forecast value |
| $M_o$ | Normalized observed value |
| $n$ | Number of cases |
| $n^*$ | A nondimensional constant (0.5) |
| $u, v$ | Horizontal wind components (m $s^{-1}$) |
| $q_s$ | Surface specific humidity (g $kg^{-1}$) |
| $S$ | Shear ($s^{-1}$) |
| $S'$ | Saturation water content for a canopy surface (2 mm) |
| $T_s$ | Skin temperature (°C) |
| $u_*$ | Surface friction velocity (m $s^{-1}$) |
| $w_s$ | Velocity scale of the boundary layer (m $s^{-1}$) |
| $\gamma_\theta$ | The countergradient term for potential temperature |
| $\rho_o$ | Air density at the surface (kg $m^{-3}$) |
| $\sigma_b$ | Stefan–Boltzman constant ($5.7 \times 10^{-8}$ W $m^{-2}$ $K^{-4}$) |
| $\sigma_f$ | Plant shading factor (between 0 and 1) |
| $\theta_o$ | Potential temperature at the first model level (°C) |
| $\theta_s$ | Surface potential temperature (°C) |
| $\theta_{sv}$ | Surface virtual potential temperature (°C) |
| $\Theta$ | Volumetric water content |

## REFERENCES

Avissar, R., and R. A. Pielke, 1989: A parameterization of heterogeneous land surfaces for atmospheric numerical models and its impact on regional meteorology. *Mon. Wea. Rev.*, **117,** 2113–2136.

Black, T. L., 1994: The new NMC mesoscale eta model: Description and forecast examples. *Wea. Forecasting*, **9,** 265–278.

Burk, S. D., and W. T. Thompson, 1992: Airmass modification over the Gulf of Mexico: Mesoscale model and airmass transformation model forecasts. *J. Appl. Meteor.*, **31,** 925–937.

Businger, J. A., J. C. Wyngaard, Y. Izumi, and E. F. Bradley, 1971: Flux-profile relationships in the atmospheric surface layer. *J. Atmos. Sci.*, **28,** 181–189.

Crisp, C. A., and J. M. Lewis, 1992: Return flow in the Gulf of Mexico. Part I: A classificatory approach with a global historical perspective. *J. Appl. Meteor.*, **31,** 868–881.

Deardorff, 1972: Parameterization of the planetary boundary layer for use in general circulation models. *Mon. Wea. Rev.*, **100,** 93–106.

——, 1973: The use of subgrid transport equations in a three-dimensional model of atmospheric turbulence. *J. Fluid Eng.*, **95,** 429–438.

Foth, H. D., and J. W. Schafer, 1980: *Soil Geography and Land Use.* J. Wiley and Sons, 484 pp.

Holtslag, A. A. M., 1987: Surface fluxes and boundary layer scaling: Model and applications. KNMI Sci. Rep. W.R. 87-02, 173 pp. [Available from KNMI, 3730 De Bilt, the Netherlands.]

——, and A. C. M. Beljaars, 1989: Surface flux parameterization schemes. KNMI Sci. Rep. W.R. 89-02, 14 pp. [Available from KNMI, 3730 De Bilt, the Netherlands.]

——, E. I. F. De Bruin, and H.-L. Pan, 1990: A high resolution airmass transformation model for short-range weather forecasting. *Mon. Wea. Rev.*, **118,** 1561–1575.

Janish, P. R., and S. W. Lyons, 1992: NGM performance during cold-air outbreaks and periods of return-flow over the Gulf of Mexico with emphasis on moisture field evolution. *J. Appl. Meteor.*, **31,** 995–1017.

Kara, A. B., 1995: A user's guide to FSU one-dimensional planetary boundary layer model. Department of Meteorology, The Florida State University, 92 pp. [Available from Department of Meteorology, The Florida State University, Tallahassee, FL 32306-4520.]

——, 1996: Boundary layer structure over and around the Gulf of Mexico. M.S. thesis, Department of Meteorology, The Florida State University, 96 pp. [Available from Department of Meteorology, The Florida State University, Tallahassee, FL 32306-4520.]

——, and J. B. Elsner, 1999: Characteristics of atmospheric boundary layer for coastal and inland locations around the Gulf of Mexico. *Atmósfera*, **12,** 1–13.

——, ——, and P. H. Ruscher, 1998a: Physical mechanism for the

Tallahassee, Florida, minimum temperature anomaly. *J. Appl. Meteor.,* **37,** 101–113.
——, A. Tribble, and P. H. Ruscher, 1998b: Effects of roughness length on the FSU one-dimensional atmospheric boundary layer model forecasts. *Atmósfera,* **11,** 239–256.
Lewis, J. M., and A. C. Crisp, 1992: Return flow in the Gulf of Mexico. Part II: Variability in return-flow thermodynamics inferred from trajectories over the gulf. *J. Appl. Meteor.,* **31,** 868–881.
——, and W. J. Martin, 1996: Estimation of the Bowen ratio over the Gulf of Mexico's continental shelf using buoy data. Preprints, *Conf. on Coastal Oceanic and Atmospheric Prediction,* Atlanta, GA, Amer. Meteor. Soc., 287–289.
——, ——, and N. L. Guinasso Jr., 1997: Bowen ratio estimates in return flow over the Gulf of Mexico. *J. Geophys. Res. (Oceans),* **102** (C5), 10 535–10 544.
Louis, J.-F., M. Tiedtke, and J. F. Geleyn, 1982: A short history of the operational PBL—Parameterization of ECMWF. Preprints, *Workshop on Planetary Boundary Layer Parameterization,* Shinfield Park, Reading, Berkshire, United Kingdom, European Centre for Medium-Range Weather Forecasts, 59–79.
Mahrt, L., 1987: Grid-averaged surface fluxes. *Mon. Wea. Rev.,* **115,** 1550–1560.
——, and M. Ek, 1984: The influence of atmospheric stability on potential evaporation. *J. Climate Appl. Meteor.,* **23,** 222–234.
——, and H.-L. Pan, 1984: A two-layer model of soil hydrology. *Bound.-Layer Meteor.,* **29,** 1–20.
Merrill, R. T., 1992: Synoptic analysis of the GUFMEX return-flow event of 10–12 March 1988. *J. Appl. Meteor.,* **31,** 849–867.
O'Brien, J. J., 1970: A note on the vertical structure of the eddy exchange coefficient in the planetary boundary layer. *J. Atmos. Sci.,* **27,** 1213–1215.
Pan, H.-L, and L. Mahrt, 1987: Interaction between soil hydrology and boundary layer development. *Bound.-Layer Meteor.,* **38,** 185–202.
Reiff, J., D. Blaauboer, H. A. R. De Bruin, A. P. van Ulden, and G. Cats, 1984: An airmass transformation model for short-range weather forecasting. *Mon. Wea. Rev.,* **112,** 393–412.
Reynolds, R. W., 1988: A real time global sea surface temperature analysis. *J. Climate,* **1,** 75–86.
Sloan, C., 1994: An airmass transformation model for coastal environments. M.S. thesis, Department of Meteorology, The Florida State University, 108 pp. [Available from Department of Meteorology, The Florida State University, Tallahassee, FL 32306-4520.]
Stull, R. B., 1983: *An Introduction to Boundary Layer Meteorology.* Kluwer Academic, 666 pp.
Troen, I., and L. Mahrt, 1986: A simple model of the atmospheric boundary layer model: Sensitivity to surface evaporation. *Bound.-Layer Meteor.,* **37,** 129–148.
Weiss, S. J., 1992: Some aspects of forecasting severe thunderstorms during cool-season return-flow episodes. *J. Appl. Meteor.,* **31,** 964–982.
Wyngaard, J. C., and R. A. Brost, 1984: Top-down and bottom-up diffusion of a scalar in the convective boundary layer. *J. Atmos. Sci.,* **41,** 102–112.
Zhang, D., and R. A. Anthes, 1982: A high-resolution model of the planetary boundary layer—Sensivity tests and comparisons with SESAME-79 data. *J. Appl. Meteor.,* **21,** 1594–1609.
Zobler, L., 1986: A world soil file for global climate modeling. NASA Tech. Memo. 87802, 33 pp. [Available from GSFC User Services, NASA/Goddard Space Flight Center, Code 902.2, Greenbelt, MD 20771.]